The Advanced Hydrotest Facility (AHF) Large Bore Quadrupole Focusing Magnet System

Joel H. Schultz, *Member, IEEE*, T. Antaya, J. V. Minervini, A. L. Radovinsky, B. A. Smith, R. J. Camille, R. L. Myatt, A. Jason, P. Walstrom, and J. A. Waynert

***Abstract*—The Advanced Hydrotest Facility (AHF) at Los Alamos will provide proton radiography of large-scale, dynamic events. The large bore (Case II) quadrupole focusing magnets are a subsystem in this facility, consisting of four complete imaging lines with a total of eight imaging plates and 52 quadrupole magnets. Each large bore quadrupole has an inner winding diameter of 660 mm and provides a gradient of 10.4 T/m with a 300 mm field of view. Each magnet is a two-layer saddle, contained by a three cm steel shell. The conductor is a Rutherford cable, soldered into a C-shaped copper channel. The magnets are cooled by the forced-flow of two-phase helium through coolant pipes. Since the winding was calculated to absorb bursts of 0.35 J/kg irradiation, both NbTi and Nb_3Sn designs are being considered.**

***Index Terms*—Magneto-optics, magnets, quadrupoles, superconducting.**

I. Introduction

THE ADVANCED Hydrotest Facility (AHF) at Los Alamos is an advanced proton radiography system that is needed to assess the primary performance and safety of a broad range of nuclear materials through dynamic testing. It is distinguished by a very large field of view and high spatial-and-time resolution of multiframe images along several axes [1].

Multiframe radiography is achieved using eight imaging lines with smaller magnetic lenses (Case I) and four lines with larger lenses (Case II). The Case I lines have a Field of View (FOV) radius of 60 mm, while the Case II lines have a FOV radius of 150 mm. Each beam line has an illuminator and monitor lens upstream of the Sample Under Test (or "object") and two sets of (Identity) Imaging Lenses downstream of the object. The three smaller quadrupoles in the illuminator are normal copper. The illuminator expands the beam to the upstream side of the Monitor Lens, which is used for characterization of the beam illuminating the object. After each of the imaging lenses, there is an imaging "plate," allowing two "snapshots" of the sample per imaging line. Snapshots can be repeated at very high-frequency of up to 20 bunches with 200 ns spacing. The use of multiple focusing lines allows viewing of the events from several different angles and even of tomographic imaging. The magnetic optical system is described in Table I.

Manuscript received August 5, 2002. This work was supported by the U.S. Department of Energy under Contract W7405-ENG-36.

J. H. Schultz, T. Antaya, J. V. Minervini, A. L. Radovinsky, and B. A. Smith are with the M.I.T. Plasma Science and Fusion Center, Cambridge, MA 02139 USA (e-mail: jhs@psfc.mit.edu).

R. J. Camille and R. L. Myatt are with Myatt Consulting, Inc. (e-mail: myatt@earthlink.net).

A. Jason, P. Walstrom, and J. A. Waynert are with the Los Alamos National Laboratory, Los Alamos, NM 87545 USA (e-mail: ajason@lanl.gov).

Digital Object Identifier 10.1109/TASC.2003.812664

TABLE I
AHF Case I and Case II Quadrupoles

Parameter	Case I (Small Lens)	Case II (Large Lens)
No. upstream (illuminator/monitor) lines	8	4
No. downstream (imaging) lines	8	4
No. quadrupoles/doublet	2	2
No. quadrupoles/imaging lens	4	4
No. imaging lenses/line	2	2
No. quadrupoles/ upstream line	5	5
No. quadrupoles/imaging line	8	8
Total singlets, system	8	4
Total doublets, system	48	24
Total quadrupoles, system	104	52

II. Case II Quadrupoles and Cryostat

A. Quadrupole Doublet and Cryostat

Each Case II quadrupole consists of four two-layer saddle coils, using NbTi Rutherford cable-in-channel conductor [2]. Two quadrupoles are assembled as a "doublet" in a single cryostat in a focus-defocus orientation. In the design option shown, the two quadrupoles are seriesed through joints in the space between them and a single pair of leads exits through the service stack. The service stack also provides feedthroughs for the helium coolant and instrumentation lead pairs. The coils are inside a liquid helium can. Two cooling options are being considered, where the baseline is a dry, indirectly-cooled winding with coolant pipes tracing the inner surface of the can and the alternative is a flooded, liquid helium cooled magnet.

The Case II magnet and cryostat overall dimensions are shown in Fig. 1 and the concept is illustrated in Fig. 2. The major dimensions of the Case II and Case I quadrupoles are listed in Table II for purposes of comparison.

Intermediate temperature thermal shields are used around all cold surfaces. The intermediate shields are thin, steel cylinders and sheets, covered with multilayer superinsulation and cooled by forced-flow helium gas with an inlet temperature of 80 K, avoiding any asphyxiation hazard in the subterranean test cell from the use of nitrogen. The outer vacuum can consists of inner and outer steel cylinders, joined by end flanges with a central hole for the beam line.

The quadrupoles are assembled with a warm iron yoke that is narrow at the waist, allowing the closest approach of the quadrupoles to the object, and thus the highest resolution at the image. The four poles are oriented with axes at NE/SE/SW/NW, in order to maximize the field decoupling between the Case I

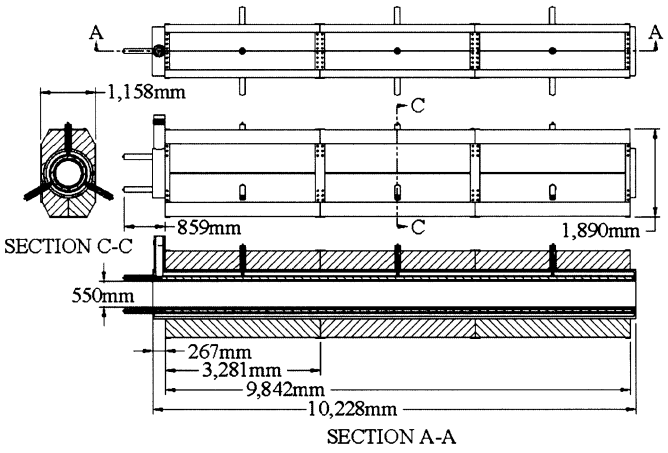

Fig. 1. Elevation, plan, and cross-section views of the Case II coil, cryostat, structure, and iron yoke.

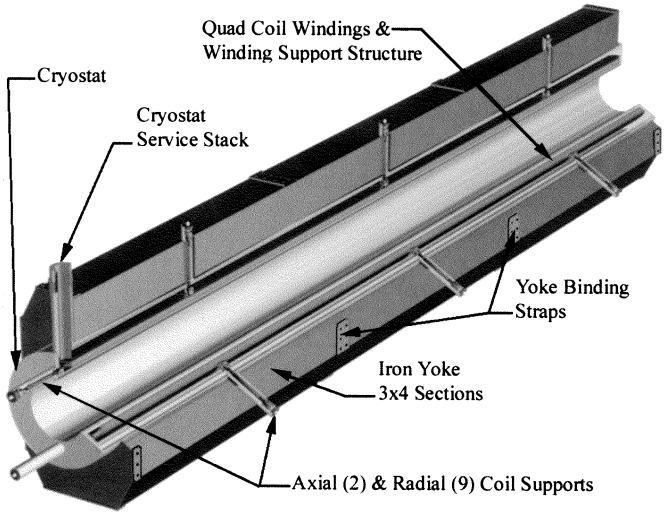

Fig. 2. Isometric cutaway of the Case II quadrupole coil, cryostat, supports, and iron yoke.

TABLE II
COMPARISON OF AHF CASE I AND II QUADRUPOLE DIMENSIONS

Parameter	Units	Case I (Small Lens)	Case II (Large Lens)
FOV radius	(mm)	60	150
$R_{inner,\ beam\ pipe}$	(mm)	114	241
$R_{inner,\ winding}$	(mm)	182	330
L_{quad}	(m)	3.1	4.25
Hard-edge equivalent quadrupole gradient	(T/m)	18.4	10.4
Winding average quadrupole gradient*	(T/m)	17.13	9.75
Total lens length	(m)	25.4	33.8

and Case II quadrupoles, despite the small iron thickness at the equator. Warm iron was selected over a cold iron yoke in order to simplify the cryostat and machine assembly. The space for both machine and utilities is restricted, being in a chamber carved out of the Los Alamos mesa.

As shown in Fig. 3, the windings are not "cos 2θ," but simply select the angles of the inner and outer layers of the winding in order to eliminate the 6th and 10th harmonics in the straight section [2]. The end turns are designed to minimize the positive and negative peaks of those harmonics, while canceling

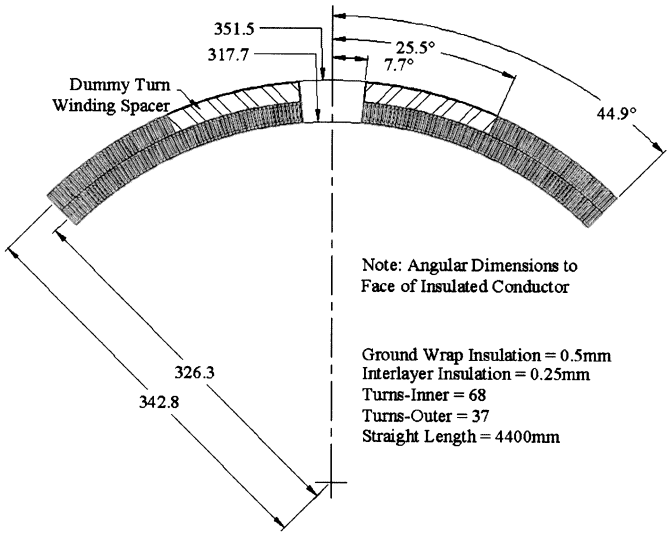

Fig. 3. Elevation, cross-section view of two layer winding and pole piece.

TABLE III
CASE II QUADRUPOLE WINDING DIMENSIONS

Parameter	Units	Value
Rinner + gndwrap	(mm)	317.7
Router + gndwrap	(mm)	351.5
tgndwrap	(mm)	0.5
tins, turn	(mm)	0.2
tins, interlayer	(mm)	0.4
nturns, inner		69
nturns, outer		37
θ_1 (pole to inner layer)	(degrees)	7.7
θ_2 (pole to outer layer)	(degrees)	25.5
NIquad	(MAT)	3.4
Bmax, center	(T)	4.28
Bmax,end turns	(T)	5.01
Wm,quadrupole	(MJ)	5.85
Lcoil	(m)	4.46
Lmagnetic	(m)	4.25

their axial integral. The spacer consists of dummy turns that are added to the outer layer to create a single structural winding arch with uniform modulus and thermal contraction. Circumferential compression in the coil pack is obtained by winding the turns on a solid core, and applying a radial precompression before welding an outer 3 cm thick stainless steel shell. The solid winding core is made of titanium, since a finite element trade study showed that a considerably lower prestress was required than with a stainless steel core [2]. There is no radial winding bobbin in the completed coil, in order to avoid dewedging forces in the winding pack radial bonding planes.

The dimensions of the winding are listed in Table III.

The conductor is a Rutherford cable in a copper C-channel, as illustrated in Fig. 4. The dimensions of the cable-in-channel are listed in Table IV. The design is based on SSC inner layer cable. The Nb_3Sn option uses the same concept of combining external copper with composite strands, but must avoid the use of solder, which would not survive the Nb_3Sn heat treatment.

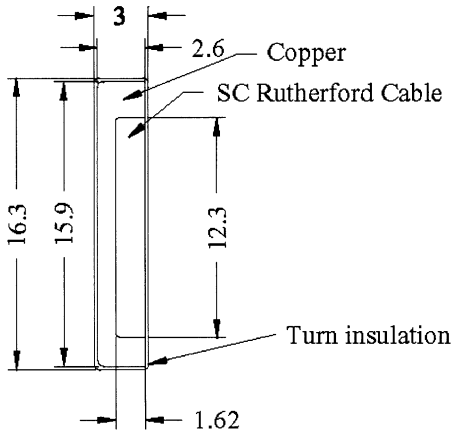

Fig. 4. Cross-section of cable-in-channel superconductor.

TABLE IV
CABLE-IN-CHANNEL CONDUCTOR DIMENSIONS

Parameter	Units	Value
h_{env}	(mm)	16.3
w_{env}	(mm)	3.0
$h_{channel}$	(mm)	15.9
$w_{channel}$	(mm)	2.6
$h_{cablespace}$	(mm)	12.3
$w_{cablespace}$	(mm)	1.623
D_{strand}	(mm)	0.808
$n_{strands}$		30
Cu/Noncu		1.3

Copper core Rutherford cable, cable-in-welded-box, and cable brazed to top/bottom plates are being considered [3]. The Nb_3Sn strand would be selected from the highly advanced candidate strands being developed for the Very Large Hadron Collider [4].

Fig. 5 shows the cold-warm gravity support concept for the cold mass. Thermal isolation is achieved by selecting the optimum length/area for the stainless steel coil support rod assembly. Relative contraction of the assembly and the cold mass during a cooldown is taken up in the bellows, which also provides a vacuum seal between the cryostat and adjusting nut volumes. The adjusting nuts are used for magnetic centering of the cold mass in the cryostat. The intermediate temperature shield to reduce radiation losses in the gravity supports is an extension of the helium cooled intermediate temperature shield of the cryostat. The attachment "ring" in the picture is actually a flexible braid, allowing relative motion between the shield and the support rod assembly. Each rod terminates in a ball and pin that are rigidly attached to each other, and that can slide along and rotate about the axis of the pin through the adapter bearing. All unbalanced magnetic forces, as well as the gravitational loads, are taken in tension or compression through the seats of the clevis pin-bearing assemblies. The top of the supported rod is seated through the nut and top washer assembly. The bottom is supported by the coil-liquid helium can adapter ring and the liquid helium can-support rod adapter ring, which is fit around

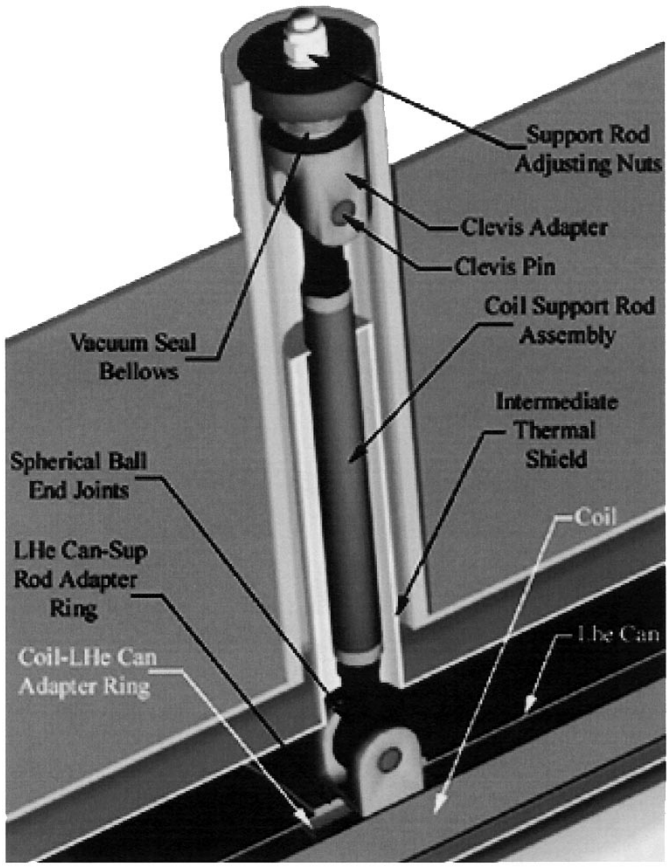

Fig. 5. Cold-warm gravity support rod assembly.

the perimeter of the coil and is one of the rings constricting radial motion of the coil. It has penetrations that allow axial helium flow.

III. DESIGN ANALYSIS

The quadrupoles provide a field gradient of 10.4 T/m, an integrated gradient-magnetic length of 44.2 T, and an FOV of 300 mm. This gives a peak field at the center of the straight leg of 4.28 T and a peak field in the end turns of 5.01 T. Although the field and gradient are modest, the $R_{bore}^2 B_o^2$ product of 2.0 m^2-T^2, corresponding to the axial force and the stored energy per unit length, are nearly three times higher than those of any previous quadrupole magnet. The implied protection and structural requirements drive the design decision to reinforce the Rutherford cable.

Because of the complexity of design with 3D partially saturated iron, independent calculations, using Vector Fields and ANSYS3D were made. The leakage field from the Case II magnets into the Case I beam is 0.45 gauss, well below the specification of 10 gauss [2]. The normalized sixth and tenth harmonics allowables are 5.0×10^{-4} and 2.0×10^{-4}, respectively; while the calculated values in the straight sections and each of the end sections are all less than 10^{-4} [2]. The iron shield introduces an octupole error that will probably require compensation.

A "2.5 D" finite element structural analysis, including axial loads on the straight section, was completed on the winding pack, steel shell, and titanium winding post. The structure was

TABLE V
CASE II QUADRUPOLE STRESSES

Structural Component	Stress Category	Unit	Stress Value	Allowable Stress
Cu Channel	Mem + Bend	MPa	200	300
	Peak	MPa	184-282-184…	$>10^4$ cycles
Turn-Wrap Insulation	Normal	MPa	182	200
	In-Plane	MPa	105	150
External Shell	Membrane	MPa	120	176
	Mem + Bend	MPa	131	310
	Peak	MPa	115-199-115…	$>10^4$ cycles

analyzed at three points, after the application of preload, after cooldown, and at full current. The winding pack and insulation are successfully kept in compression at all times through the precompression of the outer 30 mm thick stainless steel shell and the relative thermal contraction of the winding pack against the titanium core. The prestress is applied either by precompression of four shell quadrants before welding or by epoxy-filled bladders [2]. The end turns and axial structure have not yet been analyzed. The peak stresses are shown to be less than the allowables in Table V.

The most important feasibility issue with the NbTi design option is its stability against proton-beam energy. With the use of a collimator on the imaging side, Mokhov calculates that the sudden local beam-induced energy deposition in the Case II end turns is 3.12 mJ/cc [5]. Adiabatic and transient simulations calculate that the energy margin is greater than the deposition, if the superconductor fraction of the strand is greater than 0.6 [6]. However, a practical margin cannot exceed 4 mJ/cc because of the limited critical temperature of NbTi. Redesigning the conductor, using Nb_3Sn, it was calculated that the energy margin would be in the range of $50 < EM < 70$ mJ/cc for all practical copper fractions [6]. The difference between indirect and direct cooling was small in comparison to the difference between NbTi and Nb_3Sn.

Quench simulations were completed using an original quench code by Smith [2], examining the conductor options of NbTi and Nb_3Sn and the protection options of internal heaters and external dump resistors. All four options were feasible. External dump resistors were selected because of much lower boiloff, as well as lower hot spot temperature and internal voltage.

The use of Nb_3Sn presented feasibility, as well as cost problems. Since the Case II magnets cannot use the racetrack windings favored by the VLHC dipole program, there was concern that compound bends in the end turns would preclude react-and-wind, while the soldered cable-in-channel would preclude wind-and-react. A literature survey [7] indicated that wind-and-reaction of the cable-reinforcement topologies mentioned in [3] using recently developed ceramic tape, followed by vacuum-pressure impregnation, would be feasible.

IV. CONCLUSIONS

A large bore Case II quadrupole has been designed that meets all of the requirements for a 300 mm Field of View proton focusing system.

Three-dimensional field analysis shows adequate suppression of the sixth and tenth harmonics and of stray field into the Case I bore.

A support structure using a 30 mm steel shell and a titanium winding pole keeps all radial and azimuthal stresses within allowables.

The energy margin of the NbTi quadrupoles is comparable to the expected energy deposition in the magnets nearest the sample. An order of magnitude safety margin could be provided by a design using Nb_3Sn. A wind-and-react design, using ceramic fiber insulation is being developed as an alternative.

ACKNOWLEDGMENT

The authors would like to thank R. Scanlan and S. Gourlay of the Lawrence Berkeley National Laboratory, D. Chichili and G. Ambrosio of Fermilab, and J. Rice and M. Tupper of Component Technology Development for helpful discussions.

REFERENCES

[1] P. W. Lisowski and J. A. Paisner, "An advanced hydrotest facility for the stockpile stewardship program," in *Proceedings of the 4th International Topical Meeting on Nuclear Applications of Accelerator Technology*, Washington, D.C., Nov. 12–15, 2001, p. 13.

[2] J. H. Schultz *et al.*, "Advanced Hydrotest Facility (AHF) case II quadrupole design study final report," MIT Plasma Science and Fusion Center Report, PSFC/RR-02-4, Feb. 26, 2002.

[3] E. W. Collings and M.D. Sumption, "Materials, strands, and cables for superconducting accelerator magnets," Ohio State University Research Report on Grant no. DE-FG02-95ER40900, May 31, 2002.

[4] R. M. Scanlan and D. R. Dietderich, "Progress and plans for the high energy physics conductor development program," in This Conference.

[5] N. V. Mokhov and P. L. Walstrom, "Beam-lens interaction study with MARS14," Los Alamos Report LA-UR-02-0210, Feb. 10, 2002.

[6] A. L. Radovinsky, "AHF case II conductor energy margin vs. fcu, potted and He permeated designs, Nb_3Sn vs. NbTi," MIT Advanced Hydrotest Facility Report AHF-MIT-ARadovinsky-061 902-01, June 19, 2002.

[7] J. H. Schultz, "Nb_3Sn fabrication techniques and selection," MIT Advanced Hydrotest Facility Report AHF-MIT-JHSchultz-050 602-01, May 6, 2002.